ELSEVIER

Journal of Nuclear Materials 290–293 (2001) 238–244

journal of nuclear materials

www.elsevier.nl/locate/jnucmat

Modelling of erosion and deposition at limiter surfaces and divertor target plates

A. Kirschner [a,*], A. Huber [a], V. Philipps [a], A. Pospieszczyk [a], P. Wienhold [a], J. Winter [b]

[a] *Institut für Plasmaphysik, Forschungszentrum Jülich GmbH, EURATOM Association, Trilateral Euregio Cluster, D-52425 Jülich, Germany*

[b] *Institut für Experimentalphysik II, Anwendungsorientierte Plasmaphysik, Ruhr-Universität Bochum, D-44780 Bochum, Germany*

Abstract

Better understanding the processes of wall erosion and deposition remains an important issue also for future devices. The three-dimensional Monte-Carlo code ERO-TEXTOR has been developed in order to simulate plasma wall interaction and transport of eroded particles in the vicinity of wall components and to allow comparisons with experimental observations. This paper presents quantitative modelling of local transport and deposition of $^{13}CH_4$ which was injected into the edge plasma of TEXTOR-94. In addition, chemical erosion at a graphite limiter in TEXTOR is simulated. Especially, the observed CD photon emission will be compared with measurements. Finally, first results of the modelling of erosion and deposition at an ITER-like divertor target plate are presented.

Keywords: ERO-TEXTOR code; Plasma-material interaction; Erosion; Deposition; Impurity transport; Chemical erosion

1. Introduction

Understanding and control of plasma-wall interaction remains a major task also in future fusion devices like ITER [1]. Radiation losses and fuel dilution due to impurities (ITER: $Z_{\text{eff}} < 1.6$), limited lifetime of highly exposed divertors (ITER: >3000 discharges) and intolerable long-term tritium retention (ITER: <1 kg) can be crucial. These phenomena depend strongly on impurity release, local transport and redeposition which are yet not fully understood. Simulations by Brooks et al. [2] for example at divertor plates reveal high redeposition probabilities while in TEXTOR much lower values are observed. Therefore, model validation is indispensable and a detailed comparison between simulations and experiments is necessary. For this purpose the ERO-TEXTOR code was developed to simulate erosion/deposition experiments. In the following results from a $^{13}CH_4$ gas puffing experiment and spectroscopic observation of chemical erosion in TEXTOR-94 are described. The findings will be compared with ERO-TEXTOR simulations. In order to model erosion and deposition on divertor target plates, the divertor geometry has been implemented to ERO-TEXTOR. First calculations of erosion and redeposition for a carbon plate will be presented.

2. The ERO-TEXTOR code

The simulations were carried out with the three-dimensional Monte-Carlo code ERO-TEXTOR [3,4], which is a derivative of the ERO code [5]. The code describes erosion and deposition at surfaces exposed to the boundary layer of magnetically confined plasmas. Impinging ions from the background plasma erode particles by physical and chemical erosion. The released

* Corresponding author. Tel.: +49-2461 614 277; fax: +49-2461 612 660.

E-mail address: a.kirschner@fz-juelich.de (A. Kirschner).

0022-3115/01/$ - see front matter
PII: S0022-3115(00)00606-1

atoms and molecules leave the surface as neutrals. It is assumed that neutrals do not interact with the plasma and therefore move along straight lines. Ionisation and dissociation probabilities are determined at discrete locations of the trajectories resulting in ionisation/dissociation of the particles at some distance from their erosion site. Ions are driven by the forces of magnetic and electric fields and the coulomb interaction with the background plasma. The initially eroded particles have a certain probability to return to the surface where they become reflected or stick and, moreover, erode other particles. The sticking probability of atomic species is calculated by means of the TRIM [6] code or determined by input parameters in the case of molecular species due to the lack of adequate data. Particles which do not stick are treated as neutrals and the above procedure starts a new until they are either redeposited or leave the simulation volume defined by the user for reasons of computional time consumption. Deposition of carbon impurity ions from the background plasma is calculated using reflection coefficients from the TRIM database. The flux ratio to hydrogen of carbon and other impurities is determined by input parameters.

3. Local transport of externally injected methane-molecules $^{13}CH_4$

Gas puffing experiments were carried out at TEXTOR in order to study the local transport of impurities in the plasma boundary [7,8]. For that purpose a calibrated amount of methane $^{13}CH_4$ (9.2×10^{19} molecules per discharge) was puffed through a hole in an inclined limiter plate during ohmic discharges (electron temperature at the last closed flux surface $T_e = 54$ eV, ion temperature $T_i = 1.5T_e$ and electron density $n_e = 1.9\times 10^{12}$ cm^{-3}, exponential decay lengths: $\lambda_{T_{e,i}} = 40$ mm, $\lambda_{n_e} = 22$ mm). The ^{13}C marking served for discrimination deposition from the injection from ^{12}C background plasma deposition. The transport of the injected particles was observed in situ by studying their light emission pattern (CH, CII) near to the limiter surface. After total exposure of 108 s the deposits on the surface were investigated by means of ion beam analysis techniques to determine the amount and spatial distribution. Fig. 1 shows in false colours a top view of the declined plate after five $^{13}CH_4$ puffs, the ^{13}C deposition is visible as light green pattern. The thickness increments were determined after each injection in situ by colorimetry and yield a ^{13}C deposition efficiency of only $(0.2 \pm 0.1)\%$. The maximum ^{13}C layer of $\approx$100 nm is located 2–3 cm away from the puffing hole.

For the ERO-TEXTOR simulations the plasma parameters as determined by TEXTOR plasma edge diagnostics were used. The most crucial parameter in the simulations has been the sticking probability of hydrocarbon species returning to the limiter surface. The effective sticking of all neutral hydrocarbons has been set to zero ($S_{neutral} = 0$) in agreement with experimental data [9–11]. For charged hydrocarbon radicals, however, an effective sticking probability of 50% ($S_{ion} = 0.5$) has been assumed in the first attempt. This reflects the fact that charged species gain a significant amount of energy in the sheath potential resulting in a high sticking probability. Fig. 2 shows the calculated deposition pattern after the total exposure time. The distortion with respect to the toroidal axis is similar to the experimental pattern and can be explained with the $\mathbf{E} \times \mathbf{B}$ drift. Quantitative comparison, however, exhibits full disagreement since the calculated overall deposition efficiency is about 40%. This is a factor of 200 higher than the measured one. Moreover, there are significant differences in the spatial ^{13}C distribution. In the experiment the maximum of the ^{13}C distribution is located a few centimetres away from the puffing hole whereas in the simulation it is rather exactly at the location of the puffing hole (right-hand side in Fig. 2). A systematic variation of various input parameters (e.g. a change of the local plasma parameters due to the external $^{13}CH_4$ source, variation of the cross field diffusion coefficient) has been performed in order to reduce the deposition efficiency and to model the spatial ^{13}C distribution. It turned out that the sticking probability of charged hydrocarbons is the crucial parameter. The calculated ^{13}C pattern for the extreme assumption of negligible effective sticking also for charged hydrocarbons, $S_{ion} = S_{neutral} = 0$, is shown in Fig. 3. With this assumption only carbon ions contribute to the ^{13}C deposition which results in a deposition efficiency reduced by a factor of about 20 (2.5%). The remaining discrepancy can be due to uncertainties in the yield for chemical erosion for which lower limits were used, i.e. 1.5% for the formation of hydrocarbons. Moreover, CO_x formation was completely neglected. In addition to the reduced deposition efficiency the spatial ^{13}C distribution agrees now well with the experiment. As shown in Fig. 3 (right-hand side) the calculated maximum is now – similar to the experiment – located several centimetres away from the puffing hole. However, a negligible sticking of charged hydrocarbon species is difficult to imagine. The gained energy ($\approx 3T_e$) of the ions in the sheath potential should disintegrate the hydrocarbons into fragments which – according to TRIM – stick with a significant probability. It seems to be more likely to assume a large re-erosion of the freshly formed a-C:H layer instead. The effective erosion yield should be in the order of 20%.

4. Chemical erosion of a carbon test-limiter

At low electron temperatures ('cold divertor', a few eV) the yield of physical sputtering decreases. Therefore,

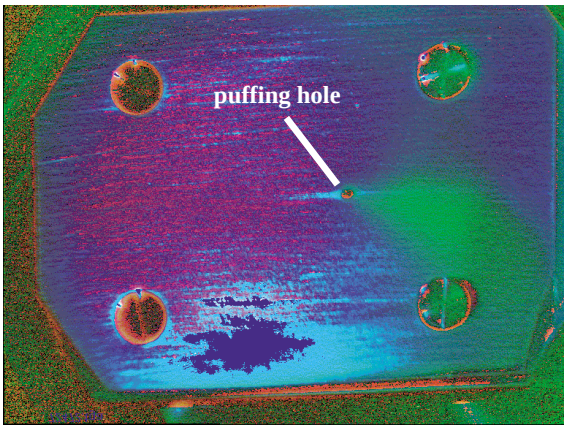

Fig. 1. False colour picture of the spatial distribution of the ^{13}C deposition resulting from five gas puffs. The deposition zone is visible as green area right from the puffing hole.

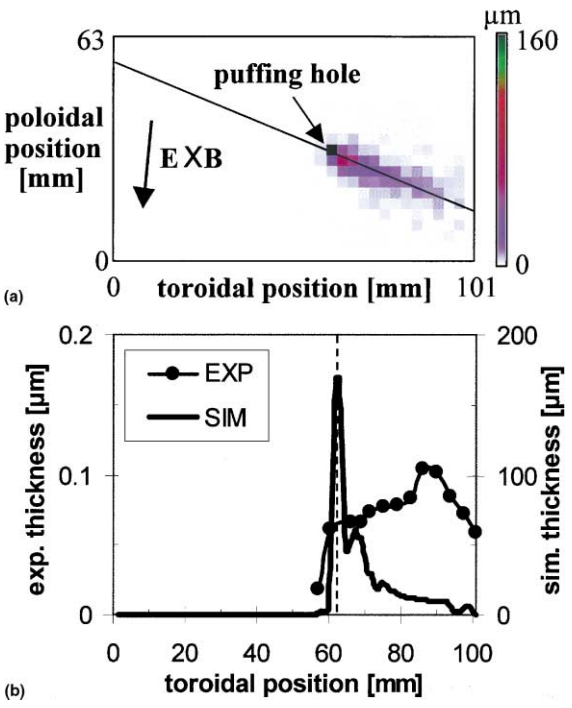

Fig. 2. Simulated ^{13}C deposition under the assumption $\mathbf{S_{ion} = 0.5}$ **and** $\mathbf{S_{neutral} = 0}$ for hydrocarbons. Left-hand side: top view of the limiter. Right-hand side: line profile along the oblique line shown in the figure to the left. The dotted line indicates the toroidal position of the puffing hole.

formation of hydrocarbons due to chemical erosion becomes the dominant erosion channel for graphite-based wall elements and determines lifetime and long-term tritium retention. A better knowledge of the

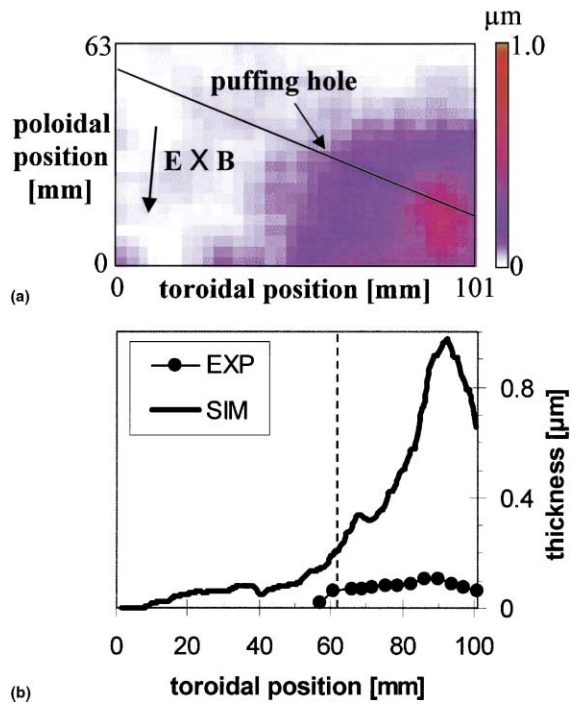

Fig. 3. Simulated ^{13}C deposition under the assumption $\mathbf{S_{ion} = S_{neutral} = 0}$ for hydrocarbons. Left-hand side: top view of the limiter. Right-hand side: line profile along the oblique line shown in the figure to the left. The dotted line indicates the toroidal position of the puffing hole.

influence of plasma and surface parameters and of local transport of hydrocarbons is thus essential.

The overall redeposition probability of chemically released methane molecules for a spherical graphite limiter exposed to typical plasma edge conditions in TEXTOR has been investigated first. As already mentioned, the assumption for the sticking probability of returning hydrocarbons is an important parameter and not well known. Fig. 4 summarises the results obtained for the usual 'standard' assumption of zero sticking for neutral and 50% sticking for charged hydrocarbons. The redeposition is integrated over the limiter surface. Input parameters for the code were T_e, $T_i = T_e$ and n_e at the LCFS and in addition the decay lengths for electron, ion temperature and density ($\lambda_{T_{e,i}} = 25$ mm and $\lambda_{n_e} =$ 20 mm). Due to decreasing penetration depths the redeposition probability increases with increasing electron density n_e and temperature T_e. Within the given parameter field, 1×10^{12} to 1×10^{13} cm^{-3} and 10–100 eV, the integrated redeposition probability is between 13% and 56%. If, however, the sticking probability of charged hydrocarbon fragments is also neglected, $S_{ion} = 0$, as has been the conclusion from the methane gas blow experiment, the redeposition drops down to

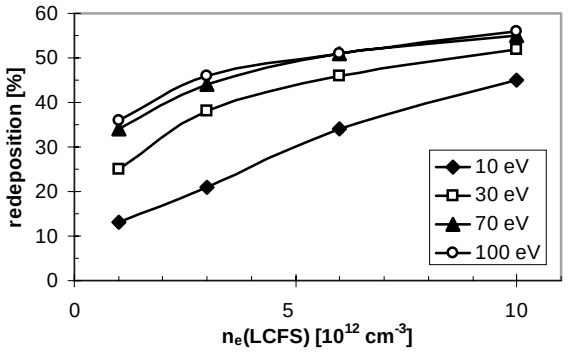

Fig. 4. Simulated redeposition probability of chemically eroded methane molecules in dependence on the electron density n_e and temperature T_e at the LCFS. Assumptions for the effective sticking of hydrocarbons: $S_{ion} = 0.5$ and $S_{neutral} = 0$.

values between 2% and 20% because it is only due to C^+ or higher ionised carbon.

Experimentally, the yield of chemical erosion can be measured from the intensity of CD emission. This intensity has to be converted with the so-called D/XB value in order to obtain the absolute amount of chemically eroded methane. The D/XB value is defined as the amount of eroded hydrocarbons related to the number of emitted CD band photons. The assumptions for the sticking of hydrocarbons should have a serious influence on the simulations. Fig. 5 shows simulated and measured [12] D/XB values in dependence on the plasma parameters for the cases of zero sticking with $S_{ion} = S_{neutral} = 0$ and of standard sticking with $S_{ion} = 0.5$ and $S_{neutral} = 0$. The measured values shown in the figure as function of the electron temperature have been obtained at different electron densities varying at the LCFS

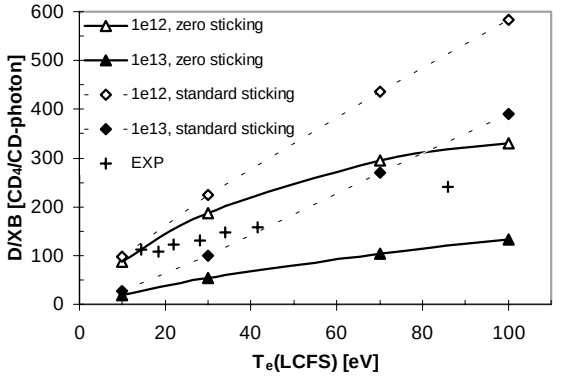

Fig. 5. Simulated and measured (EXP) D/XB values in dependence on the plasma parameters. The simulations were carried out with different assumptions for the sticking of hydrocarbons (zero sticking: $S_{ion} = S_{neutral} = 0$ and standard sticking: $S_{ion} = 0.5$, $S_{neutral} = 0$) at two electron densities $n_e(\mathrm{LCFS}) = 1 \times 10^{12}$ cm^{-3} and 1×10^{13} cm^{-3}.

between 1.4×10^{12} cm^{-3} at the highest and 3.5×10^{12} cm^{-3} at the lowest temperature. As can be seen, better agreement between simulation and experiment especially at temperatures larger than 40 eV – is obtained for the assumption of zero effective sticking for all hydrocarbons ($S_{ion} = S_{neutral} = 0$). This finding supports the conclusion drawn from the simulation calculations for the gas blow experiment.

5. Erosion and deposition at divertor target plates

Modelling calculations have been performed for a divertor target plate geometry. A relatively simple geometry is used which allows to separate the main transport effects. In toroidal direction symmetry is assumed. This simplifies the calculations such that erosion and deposition patterns have to be considered only within a poloidal stripe at the divertor plate. The temperatures $T_{e,i}$ and density n_e above the plate are described by an exponential decay towards SOL and private flux region perpendicular to the separatrix plane. The values of $T_{e,i}$ and n_e along the separatrix and the corresponding decay lengths are given by input parameters. The angle θ between separatrix and divertor plate is chosen to 20°. Fig. 6 shows a schematic view of the geometry. The electric field **E** is given by the sheath potential ($\approx 3T_e$). It is perpendicular to the divertor plate and accelerates positive charged ions to it. The direction and strength of the magnetic field are input parameters of the code. The field lines within planes parallel to the separatrix impinge with an angle of $\alpha = 2°$ relative to the divertor plate and exhibit a strength of 6 T. As can be seen in Fig. 6, the electric field **E** together with the magnetic field **B** leads to an $\mathbf{E} \times \mathbf{B}$ drift which drives positive charged ions into

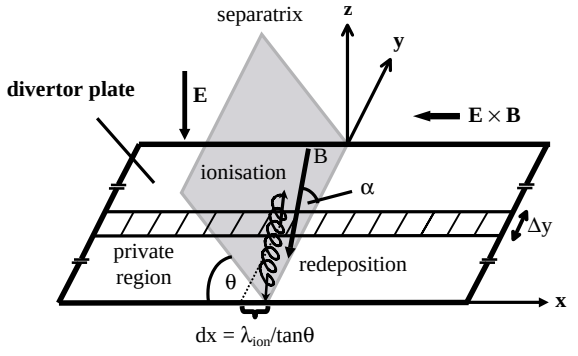

Fig. 6. Schematic representation of the simulation geometry for divertor target plates and the involved transport mechanisms. The geometry of the magnetic field results in a transport dx in positive poloidal direction, the $\mathbf{E} \times \mathbf{B}$ drift leads to a transport in negative poloidal direction.

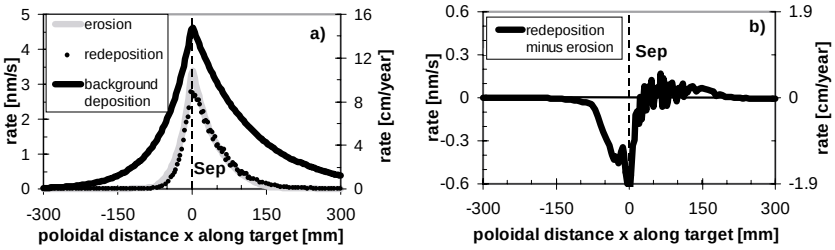

Fig. 7. (a) Profile along the plate of erosion, redeposition and deposition from the background plasma. (b) Profile of redeposition minus erosion. The profiles were simulated under consideration of physical sputtering and the plasma parameters $T_{e,i}(\mathrm{Sep}) = 12$ eV and $n_e(\mathrm{Sep}) = 1 \times 10^{14}$ cm^{-3}.

negative poloidal direction x. Besides the $\mathbf{E} \times \mathbf{B}$ drift positive charged particles are transported into positive poloidal direction x due to gyration along the magnetic field lines. As illustrated the resulting distance dx in poloidal direction between erosion and redeposition site can be approximated by

$$\mathrm{d}x = \lambda_{\mathrm{ion}} / \tan\theta \tag{1}$$

with λ_{ion} as the penetration depth of the eroded neutral. While the particle is transported in poloidal direction it of course follows the magnetic field lines also in toroidal direction and is finally redeposited outside the considered stripe (Fig. 6). This, however, is compensated by the toroidal symmetry which causes the same amount of redeposition inside the considered stripe coming from eroded particles in an according neighboured stripe.

The poloidal transport due to $\mathbf{E} \times \mathbf{B}$ drift and magnetic field forces depends on various parameters. First, the influence of physical sputtering alone is analysed. For this, an electron and ion temperature of $T_{e,i}(\mathrm{Sep}) =$ 12 eV and a density of $n_e(\mathrm{Sep}) = 1 \times 10^{14}$ cm^{-3} at the separatrix is assumed. The temperatures and density decay with a length of $\lambda_- = 3$ cm inside the private region and $\lambda_+ = 6$ cm outside. Fig. 7(a) shows the resulting profiles of erosion, redeposition and of carbon deposition from the main plasma. The relative carbon flux impinging from the main plasma on the target plate was assumed to be 1%. As can be seen this assumption leads to a carbon deposition which dominates erosion and redeposition and would lead to a continuous build up of a carbon layer. This deposition depends obviously on the flux ratio of carbon to hydrogen in the background plasma. Since this quantity is determined by global material transport currents which are out of the scope of the (local) code calculations and, moreover, there exist no clear data the carbon background deposition will further not be considered. Fig. 7(b) shows the difference of the redeposition and erosion profile. Near to the strike point ($x = 0$ mm) the erosion exceeds redeposition whereas between $x = 25$ and 150 mm a net deposition zone arises. This can be explained by the transport of eroded particles along the magnetic field lines, as discussed above, whereas the influence of the $\mathbf{E} \times \mathbf{B}$ drift is not significant under these plasma conditions. But if the temperature is increased from 12 to 40 eV at the same density of 1×10^{14} cm^{-3} the $\mathbf{E} \times \mathbf{B}$ drift becomes obvious (Fig. 8, black curve). Now, a deposition zone inside the erosion-dominated zone around the strike point arises. This is due to decreasing ionisation length λ_{ion} of sputtered carbon atoms as a result of the increased electron temperature. According to Eq. (1) the transport $\mathrm{d}x \propto \lambda_{\mathrm{ion}}$ in positive poloidal direction along the magnetic field lines is decreased and the influence of the transport in negative poloidal direction caused by the $\mathbf{E} \times \mathbf{B}$ drift becomes significant. This is true especially near to the strike point where temperature and density are highest. Here the transport is dominated by the $\mathbf{E} \times \mathbf{B}$ drift resulting in a deposition zone left to the strike point.

To demonstrate the carbon transport under the influence of chemical erosion Fig. 8 (grey curve) shows a profile of net erosion (redeposition – erosion) assuming CD_4-formation with a yield of 1%. In accordance to the results described in Sections 3 and 4 the effective sticking

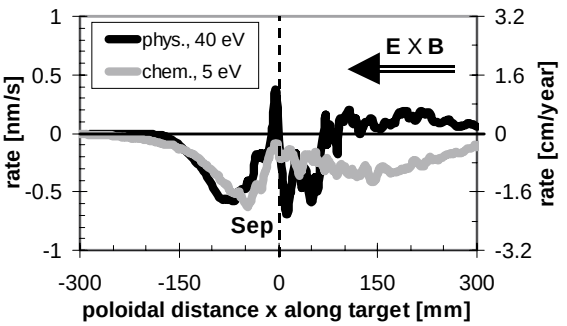

Fig. 8. Profile along the target of the difference of redeposition and erosion. Black line: physical sputtering with $T_{e,i}(\mathrm{Sep}) =$ 40 eV and $n_e(\mathrm{Sep}) = 1 \times 10^{14}$ cm^{-3}. Grey line: chemical erosion with $Y_{CD_4} = 1\%$, $T_{e,i}(\mathrm{Sep}) = 5$ eV, $n_e(\mathrm{Sep}) = 1 \times 10^{14}$ cm^{-3} and the assumption of zero sticking for hydrocarbons ($S_{\mathrm{ion}} = S_{\mathrm{neutral}} = 0$).

Table 1
Simulated integrated redeposition and net erosion in maximum in dependence on the erosion channel (physical or chemical erosion) and the plasma parameters[a]

		T_e(Sep) (eV)	Integrated redeposition (%)	Net erosion in maximum (cm/yr)
Physical sputtering		12	90	1.9
		40	98	2.4
Chemical erosion	$S_{ion} = S_{neutral} = 0$	5	74	1.9
	$S_{ion} = S_{neutral} = 0$	12	87	1.6
	$S_{ion} = 0.5$ and $S_{neutral} = 0$	5	78	1.3
	$S_{ion} = 0.5$ and $S_{neutral} = 0$	12	90	0.9

[a] In the case of chemical erosion two different assumptions for the sticking of hydrocarbons were made for comparison.

of returning hydrocarbons is set to zero ($S_{ion} = S_{neutral} = 0$). The electron temperature is chosen to $T_e(\text{Sep}) = 5$ eV and the density – as before – to $n_e(\text{Sep}) = 1 \times 10^{14}$ cm^{-3} with the former decay lengths ($\lambda_- = 3$ cm and $\lambda_+ = 6$ cm). In general the profile resembles the profile created by physical sputtering at the high electron temperature $T_e(\text{Sep}) = 40$ eV (see Fig. 8, black curve). Significant differences occur only in the absolute values of erosion and deposition: the assumed yield for chemical erosion of 1% all along the divertor plate is higher than the erosion yield due to physical sputtering, in particular far away from the strike zone where physical sputtering vanishes due to low electron temperatures. This prevents net deposition zones at these locations.

Table 1 summarises the amount of redeposition integrated over the plate and the maximal net erosion, i.e. erosion – redeposition, for different conditions (deposition from background plasma flow is always neglected). Also shown are the values, if the standard sticking assumption is used with 50% sticking for ionised hydrocarbon fragments. The electron density is kept at $n_e(\text{Sep}) = 1 \times 10^{14}$ cm^{-3} whereas the temperature varies between 5 and 40 eV. For physical sputtering the amount of redeposition reaches a value of 90% at a temperature $T_e(\text{Sep}) = 12$ eV increasing up to 98% at 40 eV. Redeposition of chemically eroded hydrocarbons is between 74% and 87% for temperatures between $T_e(\text{Sep}) = 5$ and 12 eV, respectively, using the 'zero sticking' assumption. Surprisingly, the influence of the sticking model on the integrated redeposition probability is relatively small for the divertor conditions, in contrast to the TEXTOR limiter case. Transition from zero effective sticking for charged hydrocarbons ($S_{ion} = 0$) to 50% sticking ($S_{ion} = 0.5$) results only in a moderate increase of redeposition to 78% in the case of 5 eV separatrix temperature and to 90% in the case of 12 eV. For the lifetime of divertor plates the net erosion in the maximum is the crucial parameter. Neglecting any impurity deposition from the main plasma this value varies between 0.9 and 2.4 cm/yr for the different conditions (Table 1). If the carbon fraction within the impinging plasma flow exceeds a value of about 0.2%, then the background carbon deposition will exceed the erosion at each location at the plate and therefore a carbon layer will build up.

6. Conclusion

The three-dimensional Monte-Carlo code ERO-TEXTOR has been developed to simulate plasma-wall interaction and transport of eroded particles near to limiter and divertor surfaces. Attempts to model the local pattern and amount of ^{13}C deposition from $^{13}CH_4$ gas injection through limiters in TEXTOR are best if negligible effective sticking of hydrocarbon species is assumed. This finding should be physically interpreted such that freshly deposited hydrocarbons have a very high probability to be re-eroded. The erosion yield must be about one order of magnitude higher than the usual assumptions of chemical erosion (1–3%). Simulations of experimental findings of chemical erosion at a graphite limiter come to similar conclusions. In particular the dependence of the D/XB value on the electron temperature can be best reproduced by ERO-TEXTOR assuming again $S_{ion} = S_{neutral} = 0$. The modelling of erosion and deposition at divertor plates showed that two effects influence the poloidal material transport: the $\mathbf{E} \times \mathbf{B}$ transport perpendicular to the magnetic field and the transport along the magnetic field lines. If eroded particles have short penetration lengths (in the order of mm) the $\mathbf{E} \times \mathbf{B}$-induced transport can dominate. The overall redeposition probability is between 98% and 75% with the lowest value for low temperature plasma conditions and chemical erosion as impurity production mechanism. However, lifetime of target plates is only crucial if deposition from background plasma is small. The simulations show that this could be possible if the carbon concentration within the background plasma is less than $\approx$0.2%.

References

[1] ITER Physics Basis Editors, Nucl. Fus. 39 (12) (1999).
[2] J.N. Brooks, D. Alman, G. Federici et al., J. Nucl. Mater. 266–269 (1999) 58.
[3] U. Kögler, J. Winter, ERO-TEXTOR: 3D-Monte-Carlo Code for Local Impurity Modeling in the Scrape-Off-Layer of TEXTOR-94, Jül-Report 3361, Forschungszentrum Jülich GmbH, Jülich, 1997.
[4] A. Kirschner, V. Philipps, J. Winter, U. Kögler, Nucl. Fus. 40 (5) (2000) 989.
[5] D. Naujoks, R. Behrisch, J.P. Coad, L. deKock, Nucl. Fus. 33 (4) (1993) 581.
[6] W. Eckstein, Computer Simulation of Ion–Solid Interaction, Springer, Berlin, 1991.
[7] P. Wienhold et al., these Proceedings.
[8] P. Wienhold, H.G. Esser, D. Hildebrandt et al., in: Proceedings of the 26th EPS Conference on Controlled Fusion and Plasma Physics, 14–18 June 1999, Maastricht, Netherlands.
[9] W. Möller, Appl. Phys. A 56 (1993) 527.
[10] H. Toyoda, H. Kojima, H. Sugai, Appl. Phys. Lett. 54 (1989) 1507.
[11] H. Kojima, H. Toyoda, H. Sugai, Appl. Phys. Lett. 55 (1989) 1292.
[12] A. Pospieszczyk, V. Philipps, E. Casarotto et al., J. Nucl. Mater. 241–243 (1997) 833.